DOI:10.1190/segam2020-3426813.1

# Joint Gramian inversion of geophysical data with different resolution capabilities

*Xiaolei TU[1*] and Michael S. Zhdanov[1,2]; [1]University of Utah; [2]TechnoImaging*

**Summary**

Joint inversion of multiphysics data is a practical approach to the integration of geophysical data, which produces models of reduced uncertainty and improved resolution. The development of effective methods of joint inversion requires considering different resolutions of different geophysical methods. This paper presents a new framework of joint inversion of multiphysics data, which is based on Gramian constraints and mitigates the difference in resolution capabilities of different geophysical methods. Our method enforces structural similarity between different model parameters through minimizing a structural Gramian term and it also balances the different resolutions of geophysical methods using a multiscale resampling strategy. The effectiveness of the proposed method is demonstrated by synthetic model study of joint inversion of the P-wave traveltime and gravity data.

**Introduction**

Joint inversion of multiphysics data is an effective approach to mitigate the non-uniqueness of geophysical inverse problems and to reduce the uncertainties of inverse models (Zhdanov et al., 2012). It applies constraints through complementing each dataset with information derived from the other datasets. The different physical fields are sensitive to different properties and exhibit different sensitivity patterns as a result of their different governing physical laws. We could, therefore, harness the complementary sensitivity to produce geophysical models of the subsurface target with reduced uncertainty.

Several approaches to joint inversion have been developed over the last decades. They can be classified into two categories, namely, petrophysical and structural approaches. The former correlates different physical parameters via a theoretical, empirical, or statistical petrophysical relationship (e.g., Sun and Li, 2016; 2015; Nielsen and Jacobsen, 2000; Giraud et al., 2017; Afnimar et al., 2002; Gao et al., 2012). The latter enforces the models of different physical properties to have similar spatial structures (e.g., Gallardo and Meju, 2004; 2007; Roux et al., 2011). The majority of the aforementioned methods, however, do not consider different resolution capabilities of different geophysical methods while representing models of different physical parameters with the same discretization mesh. The resolution capabilities of geophysical methods often differ significantly from each other due to different factors, such as data coverage, subsurface geology, the physical nature of geophysical field, etc. Ignoring the resolution issue may lead to (1) data fitting issues; (2) artifacts of unreasonable fine (i.e., too good to be true) structures for model parameters corresponding to methods with low-resolution capabilities; and (3) slow convergence behavior of the joint inversion iteration process (Heincke et al., 2017). A challenging but essential issue for joint inversion is to account for the resolution difference in a unified inversion regime without biased model parameterization.

We propose a new framework for joint inversion of multiphysics data based on the Gramian constraint (Zhdanov et al., 2012). Our method could (1) enforce structural similarity between different model parameters through minimizing a structural Gramian term, and (2) honor the different resolution capabilities of different geophysical methods with a multiscale resampling strategy. We have demonstrated the effectiveness of the proposed method with synthetic models by jointly inverting the P-wave traveltime and gravity data.

**Forward modeling**

The gravity field is calculated by the integral representation of the gravitational field with the point mass approximation method (Cuma et al., 2012; Zhdanov, 2015). We solve the isotropic eikonal equation for seismic traveltimes. A grid-based solver, namely the multistage fast marching (FMM) method, is employed to solve the eikonal equation (De Kool et al., 2006; Rawlinson et al., 2006). The forward modeling problems could be represented in matrix form as follows:

$$\mathbf{d}^{(i)} = \mathbf{A}^{(i)}\left(\mathbf{m}^{(i)}\right), i = 1,2; \quad (1)$$

where $\mathbf{d}^{(1)}$ and $\mathbf{d}^{(2)}$ represent the column vectors of gravity and seismic traveltime data; $\mathbf{m}^{(1)}$ and $\mathbf{m}^{(2)}$ denote vectors of subsurface density and P-wave velocity models; $\mathbf{A}^{(1)}$ and $\mathbf{A}^{(2)}$ denote the forward operators for gravity field and seismic traveltimes, respectively.

**Joint inversion methodology**

*A. Parameterization*

To address the issue of different resolution capabilities, we decouple the forward modeling meshes for different physical properties. Seismic waves usually have better resolution than the gravity field. We, therefore, set the velocity to mesh much finer than density mesh for forward modeling, so that the details of the velocity model could be sampled by seismic waves and that the density model is not oversampled. In order to jointly invert seismic and gravity data, the velocity and density models should be coupled at the same scale, especially if the structural resemblance between them is considered. In this case, we should match the long-



10.1190/segam2020-3426813.1

wavelength structures only of the velocity model with the density model, as the fine structures of short wavelength are beyond the resolution of the gravity field. A parameterization scheme enabling multiscale resampling of the model parameters is desirable.

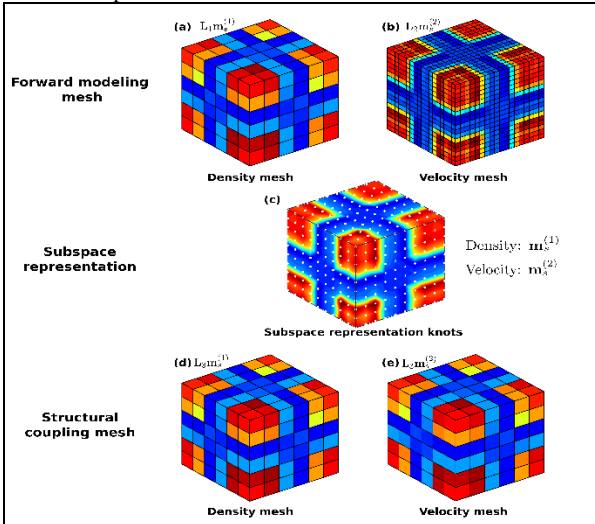


Figure 1: Schematic representation of the multiscale resampling of the density and velocity models for forward modeling and structural coupling. The density and velocity models are assumed to be represented by cubic B-spline functions. The white dots in panel (c) denote the knots of the subspace representation. The models are resampled by a coarse mesh (a) and a fine mesh (b) to honor the different resolution capabilities of gravity and seismic data. The models are resampled at the same third mesh to facilitate the structural coupling between them (panels (d) and (e)). This mesh is coarser than or the same as mesh (a) so that only the long wavelength structures of velocity model are preserved and matched with density model.

In a general case, we can represent the spatial variations of density and velocity by projecting them to the associated interpolant-type subspace. Cubic B-spline interpolant is particularly prevalent in geophysics since it offers $C^2$ continuity, local control, and the potential for an irregular distribution of knots (Rawlinson et al., 2008). Any model, $\mathbf{m}$, in the original high-dimensional space can be represented uniquely as a linear combination of the cubic spline functions (basis) as follows:

$$\mathbf{m} = \mathbf{L}\mathbf{m}_s, \tag{2}$$

where $\mathbf{m}_s$ denotes a vector in the subspace with its elements defined discretely at the knot positions; $\mathbf{L}$ is the matrix constituted of cubic B-spline functions. $\mathbf{L}$ is controlled by the knots and resampling mesh. The action of $\mathbf{L}$ to vector $\mathbf{m}_s$ would resample the model to the corresponding mesh.

As illustrated in Figure 1, the models are resampled at three scales with three meshes. For forward modeling, we resample the density model with a coarse mesh (a), and the velocity model with a fine mesh (b). The third coarse mesh is employed to resample both the density and velocity models so that they are coupled at the same scale, (d) and (e). The third mesh should not be finer than the coarse mesh (a) so that only the long-wavelength structures resolvable by gravity field are matched between density and velocity models. We set it the same as mesh (a) in Figure 1 for simplicity.

### *B. Gramian based structural coupling*

A fundamental issue of joint inversion is to define an appropriate coupling term. We use a structural coupling based on the Gramian constraint (Zhdanov et al., 2012; Zhdanov, 2015):

$$s\left(\mathbf{m}_\mathbf{s}^{(1)}, \mathbf{m}_\mathbf{s}^{(2)}\right) = \iiint_D g\left(\nabla\left(\mathbf{T}^{(1)}\mathbf{L}_3\mathbf{m}_\mathbf{s}^{(1)}\right), \nabla\left(\mathbf{T}^{(2)}\mathbf{L}_3\mathbf{m}_\mathbf{s}^{(2)}\right)\right) dv\,, \tag{3}$$

where $\nabla = \left[\nabla_x, \nabla_y, \nabla_z\right]^T$ denotes the gradient operator. The operators $\mathbf{T}^{(1)}$ and $\mathbf{T}^{(2)}$ transform the models into another space. In our synthetic study, we transform velocity to velocity perturbation to promote structural resemblance between velocity perturbation and density. The matrix of cubic B-spline basis, $\mathbf{L}_3$, resamples the models with the same coarse mesh so that the two models are coupled at the same scale. Symbol $g(\,,\,)$ represents the Gramian (i.e., the determinant of the Gram matrix) of the gradient at a single point:

$$g\left(\nabla\left(\mathbf{T}^{(1)}\mathbf{L}_3\mathbf{m}_\mathbf{s}^{(1)}\right), \nabla\left(\mathbf{T}^{(2)}\mathbf{L}_3\mathbf{m}_\mathbf{s}^{(2)}\right)\right) = \begin{vmatrix} \left(\nabla\left(\mathbf{T}^{(1)}\mathbf{L}_3\mathbf{m}_\mathbf{s}^{(1)}\right), \nabla\left(\mathbf{T}^{(1)}\mathbf{L}_3\mathbf{m}_\mathbf{s}^{(1)}\right)\right) & \left(\nabla\left(\mathbf{T}^{(1)}\mathbf{L}_3\mathbf{m}_\mathbf{s}^{(1)}\right), \nabla\left(\mathbf{T}^{(2)}\mathbf{L}_3\mathbf{m}_\mathbf{s}^{(2)}\right)\right) \\ \left(\nabla\left(\mathbf{T}^{(2)}\mathbf{L}_3\mathbf{m}_\mathbf{s}^{(2)}\right), \nabla\left(\mathbf{T}^{(1)}\mathbf{L}_3\mathbf{m}_\mathbf{s}^{(1)}\right)\right) & \left(\nabla\left(\mathbf{T}^{(2)}\mathbf{L}_3\mathbf{m}_\mathbf{s}^{(2)}\right), \nabla\left(\mathbf{T}^{(2)}\mathbf{L}_3\mathbf{m}_\mathbf{s}^{(2)}\right)\right) \end{vmatrix}, \tag{4}$$

where $(\,,\,)$ denotes the inner product. The Gramian, $\boldsymbol{g}$, is nonnegative and it is zero if and only if the two gradient vectors are parallel. Therefore, by minimizing $\boldsymbol{g}$, we would enforce the gradient vectors of the model parameters to be mutually parallel at a specific subsurface position.

It could be demonstrated that the Gramian $\boldsymbol{g}$ is equal to the $L_2$ norm of the cross-gradient term (Gallardo and Meju, 2004; 2007):

$$\boldsymbol{g}\left(\nabla\boldsymbol{m}^{(1)}(\mathbf{r}), \nabla\boldsymbol{m}^{(2)}(\mathbf{r})\right) = \left\|\nabla\boldsymbol{m}^{(1)}(\mathbf{r}) \times \nabla\boldsymbol{m}^{(2)}(\mathbf{r})\right\|^2. \tag{5}$$

The Gramian, however, is (1) easier to implement due to its quadratic form, similar to L2 norm stabilizers; (2) more convenient to be incorporated in optimization; (3) more flexible for manipulation of the model parameters in different transformed spaces; and (4) more flexible to incorporate data of different resolution capabilities.

The structural coupling term, $\boldsymbol{s}\left(\mathbf{m}_\mathbf{s}^{(1)}, \mathbf{m}_\mathbf{s}^{(2)}\right)$, in Eq. (3) is an integral (superposition) of the nonnegative Gramians. It would be minimized only if the Gramians, $\boldsymbol{g}$, are all

DOI:10.1190/segam2020-3426813.1

minimized at every subsurface position, leading to zero Gramians and consequently mutually parallel gradient vectors everywhere in the whole inversion domain, $\boldsymbol{D}$. As with the cross-gradient method, aligned gradient orientations of different model parameters necessitate the coincidence of structural boundaries of them.

*C. Objective functional*

The joint inversion of gravity and seismic traveltime data is performed by minimizing the objective functional (Zhdanov, et al., 2012; Zhdanov, 2015):

$$p = \sum_{i=1}^{2} \Phi^{(i)}\left(\mathbf{m}_s^{(i)}\right) + \sum_{i=1}^{2} \alpha^{(i)}\Psi^{(i)}\left(\mathbf{m}_s^{(i)}\right) + \beta s\left(\mathbf{m}_s^{(1)}, \mathbf{m}_s^{(2)}\right), \quad (6)$$

where $\Phi^{(i)}$ denotes the misfit functional for the $i$-th type of data; $\Psi^{(i)}$ represents the regularization stabilizer promoting preferred structures of the model; $s\left(\mathbf{m}_s^{(1)}, \mathbf{m}_s^{(2)}\right)$ is the joint stabilizer enforcing structural coupling. $\alpha^{(i)}$ and $\beta$ are the regularization parameters balancing the misfits and the corresponding stabilizers.

As the probability density functions of data and model uncertainties are usually characterized by long-tailed distribution (Claerbout and Muir, 1973), the least-squares ($L_2$ norm) error metric based on Gaussian uncertainty assumption often leads to biased models (Tarantola, 2005). Error metrics less sensitive to large measurement errors and more appropriate to long-tailed probability density functions could yield far more stable estimation of the model parameters than L2 norm (Guitton and Symes, 2003). We employ the robust norms for the misfit functional:

$$\Phi^{(i)}\left(\mathbf{m}_s^{(i)}\right) = \left\| \mathbf{W}_d^{(i)}\left[\mathbf{A}^{(i)}\left(\mathbf{L}_i\mathbf{m}_s^{(i)}\right) - \mathbf{d}^{(i)}\right]\right\|_\rho^2, \quad (7)$$

where $\mathbf{W}_d^{(i)}$ represents the corresponding data weighting matrix; $\mathbf{d}^{(i)}$ is the observed data, i.e., gravity data or P-wave first arrivals; $\| \quad \|_\rho^2$ denotes the robust norm, e.g., Huber or Bisquare norm. The robust norms could be easily represented as quasi-quadratic functionals (Zhdanov, 2015; Tu and Zhdanov, 2020), making it convenient to optimize.

The general methods of solving the above inverse problems were developed in Zhdanov (2015). We base our solution on the re-weighted regularized conjugate gradient method (RRCG), which is easier to implement numerically. Implementation details of the RRCG method for joint inversion problems could be found in Zhdanov et al. (2012), Zhu (2017), and Lin and Zhdanov (2019 (b)).

**Model study**

The developed method was tested using computer-generated data. Model 1 represents a homogeneous half-space containing four blocky. Figure 2 presents horizontal sections of the true density contrast and velocity perturbation at a depth of 10 $km$. The density distribution inside each anomaly is homogeneous and even. The corresponding velocity perturbation was designed to exhibit fine patterns, which could be resolved by the seismic waves while beyond the resolution capability of the gravity field. Four tiny ball-shaped high velocity anomalies with radius of 1 $km$ were also set for the velocity model at a depth of 20 $km$. There is no density anomaly at positions corresponding to the four tiny high-velocity balls. The background P-wave velocity of the half-space is 6 $km/s$. A joint gravity and seismic survey consisting of 484 gravity stations and 225 seismic stations were designed to map the anomalies. The distribution of earthquake epicenters and gravity and seismic stations are also shown in Figure 2. The computer-simulated gravity data were contaminated with random noise with a standard derivation of 0.1 $mGa$, which corresponds to a relative noise level of 3.6% . The computed traveltimes also contain random noise with a level of 7 $ms$ (i.e., 5%).

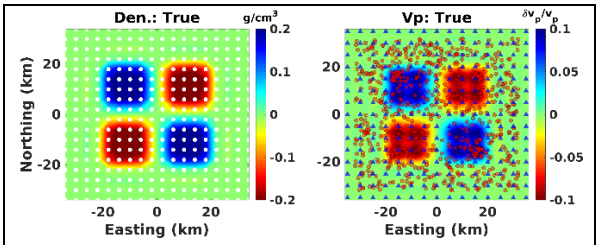


Figure 2: Horizontal sections of true density and velocity model at a depth of 10 km. The white dotes denote gravity stations. The red dots are earthquake epicenters. The seismic stations are represented by blue triangles.

Table 1: Inversion setup with multiscale resampling

| Knot/mesh | Interval/cell size East × North × Depth | Num. of knots/Cells East × North × Depth |
|---|---|---|
| Subspace representation | 4 km × 4 km × 2 km | 21 × 21 × 16 |
| Density: forward modeling | 4 km × 4 km × 2 km | 18 × 18 × 13 |
| Velocity: forward modeling | 1 km × 1 km × 1 km | 73 × 73 × 27 |
| Structural coupling | 4 km × 4 km × 2 km | 18 × 18 × 13 |

We first inverted the gravity and seismic traveltime data separately using the RRCG method with MN stabilizer (Zhdanov, 2015). The same data were then jointly inverted using the developed method with multiscale resampling setups shown in Table 1. The knot/mesh setups for the separate inversions are the same as for joint inversion. Comparisons of the true and inverted models are presented in Figure 3. The joint inversion recovers the density model much better compared to separate inversion. The artifacts in the velocity model are also significantly reduced in joint inversion. The joint inversion produces models with



10.1190/segam2020-3426813.1

improved structural similarity and better-aligned density and velocity gradients. Most importantly, by using the multiscale resampling, the joint inversion does not introduce artifact of over coupling to the density model.

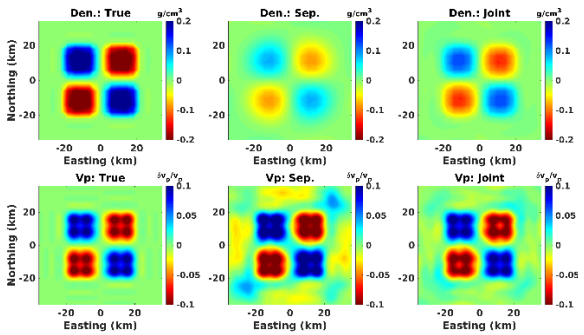


Figure 3: Horizontal sections of true, separately, and jointly inverted models ata depth of 10 $km$.

For comparison, we then ran the same joint inversion with the same structural coupling method but without multiscale resampling. The inversion setups are shown in Table 2. The gravity and seismic traveltime data were modeled with the same fine mesh, and the density and velocity models were structurally coupled with the same mesh. The inverted models are shown in Figure 4. Both jointly inverted density and velocity models show significant improvement compared to the separately inverted ones. The fine structures inside each anomaly are also observed in the jointly recovered density model, which, however, are too good to be true, since such fine-scale structures are beyond the resolution of the gravity data.

Table 2: Inversion setups without multiscale resampling

| Knot/mesh | Interval/cell size East × North × Depth | Num. of knots/Cells East × North × Depth |
|---|---|---|
| Subspace representation | 4 km × 4 km × 2 km | 21 × 21 × 16 |
| Density: forward modeling | 1 km × 1 km × 1 km | 73 × 73 × 27 |
| Velocity: forward modeling | 1 km × 1 km × 1 km | 73 × 73 × 27 |
| Structural coupling | 1 km × 1 km × 1 km | 73 × 73 × 27 |

The jointly inverted density and velocity models are structurally coupled at both long and short wavelength scale, leading to fine-scale artifacts in the density model. Especially at a depth of 20 $km$, the four tiny ball-shaped anomalies are also presented in the density model as a result of over coupling. The joint inversion results with multiscale resampling, however, are free of such over coupling artifacts, which demonstrates the importance of accounting for the difference of resolution capabilities of different geophysical methods in joint inversion.

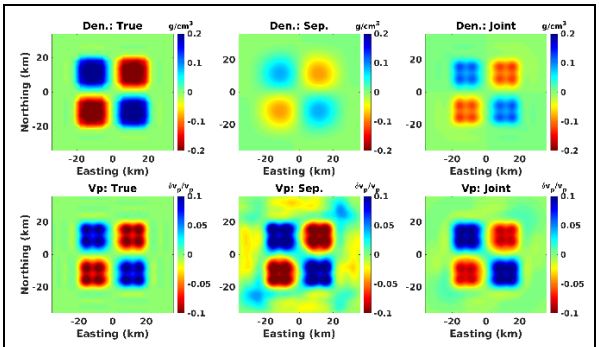


Figure 4: Horizontal sections of true, separately and jointly inverted models at the depth of 10 $km$.

## Conclusions

We have developed a framework for joint inversion of multiphysics data based on the Gramian constraint. Our method promotes structural similarity between different physical parameters by minimizing a Gramian based structural coupling term. These structural constraints could be considered as a generalization of the cross-gradient method. The quadratic nature of the Gramian structural coupling term makes it numerical implementation similar to conventional L2 norm stabilizing functionals.

The developed method could also consider the differences in resolution capabilities of different geophysical methods using a multiscale resampling strategy. The effectiveness of the method was shown by jointly inverting the P-wave traveltime and gravity data. Our synthetic model study demonstrated that joint inversion without considering the resolution differences might result in creating artifacts in the inverse models. Thus, the developed method successfully avoids the over coupling problem.

## Acknowledgments

We are thankful to the Consortium for Electromagnetic Modeling and Inversion at the University of Utah, and TechnoImaging for supporting this research.

## REFERENCES


Afnimar, A., K. Koketsu, and K. Nakagawa, 2002, Joint inversion of refraction and gravity data for the three-dimensional topography of a sediment–basement interface: Geophysical Journal International, **151**, 243–254, doi: https://doi.org/10.1046/j.1365-246X.2002.01772.x.

Claerbout, J. F., and F. Muir, 1973, Robust modeling with erratic data: Geophysics, **38**, 826–844, doi: https://doi.org/10.1190/1.1440378.

Čuma, M., G. A. Wilson, and M. S. Zhdanov, 2012, Large scale 3D inversion of potential field data: Geophysical Prospecting, **60**, 1186–1199, doi: https://doi.org/10.1111/j.1365-2478.2011.01052.x.

de Kool, M., N. Rawlinson, and M. Sambridge, 2006, A practical grid-based method for tracking multiple refraction and reflection phases in three-dimensional heterogeneous media: Geophysical Journal International, **167**, 253–270, doi: https://doi.org/10.1111/j.1365-246X.2006.03078.x.

Gallardo, L. A., and M. A. Meju, 2004, Joint two-dimensional DC resistivity and seismic travel time inversion with cross-gradients constraints: Journal of Geophysical Research: Solid Earth, **109**, doi: https://doi.org/10.1111/j.1365-246X.2007.03366.x.

Gallardo, L. A., and M. A. Meju, 2007, Joint two-dimensional cross-gradient imaging of magnetotelluric and seismic traveltime data for structural and lithological classification: Geophysical Journal International, **169**, 1261–1272, doi: https://doi.org/10.1111/j.1365-246X.2007.03366.x.

Gao, G., A. Abubakar, and T. M. Habashy, 2012, Joint petrophysical inversion of electromagnetic and full-waveform seismic data: Geophysics, **77**, no. 3, WA3–WA18, doi: https://doi.org/10.1190/geo2011-0157.1.

Giraud, J., E. Pakyuz-Charrier, M. Jessell, M. Lindsay, R. Martin, and V. Ogarko, 2017, Uncertainty reduction through geologically conditioned petrophysical constraints in joint inversion: Geophysics, **82**, no. 6, ID19–ID34, doi: https://doi.org/10.1190/geo2016-0615.1.

Guitton, A., and W. W. Symes, 2003, Robust inversion of seismic data using the Huber norm: Geophysics, **68**, 1310–1319, doi: https://doi.org/10.1190/1.1598124.

Heincke, B., M. Jegen, M. Moorkamp, R. W. Hobbs, and J. Chen, 2017, An adaptive coupling strategy for joint inversions that use petrophysical information as constraints: Journal of Applied Geophysics, **136**, 279–297, doi: https://doi.org/10.1016/j.jappgeo.2016.10.028.

Lin, W., and M. S. Zhdanov, 2018, Joint multinary inversion of gravity and magnetic data using Gramian constraints: Geophysical Journal International, **215**, 1540–1557, doi: https://doi.org/10.1093/gji/ggy351.

Nielsen, L., and B. H. Jacobsen, 2000, Integrated gravity and wide-angle seismic inversion for two-dimensional crustal modelling: Geophysical Journal International, **140**, 222–232, doi: https://doi.org/10.1046/j.1365-246x.2000.00012.x.

Rawlinson, N., and M. Sambridge, 2004, Wave front evolution in strongly heterogeneous layered media using the fast marching method: Geophysical Journal International, **156**, 631–647, doi: https://doi.org/10.1111/j.1365-246X.2004.02153.x.

Rawlinson, N., J. Hauser, and M. Sambridge, 2008, Seismic ray tracing and wavefront tracking in laterally heterogeneous media: Advances in Geophysics, **49**, 203–273.

Roux, E., M. Moorkamp, A. G. Jones, M. Bischoff, B. Endrun, S. Lebedev, and T. Meier, 2011, Joint inversion of long-period magnetotelluric data and surface-wave dispersion curves for anisotropic structure: Application to data from Central Germany: Geophysical Research Letters, **38**, doi: https://doi.org/10.1029/2010GL046358.

Sun, J., and Y. Li, 2016, Joint inversion of multiple geophysical data using guided fuzzy c-means clustering: Geophysics, **81**, no. 3, ID37–ID57, doi: https://doi.org/10.1190/geo2015-0457.1.

Tarantola, A., 2005, Inverse problem theory and methods for model parameter estimation: Society for Industrial and Applied Mathematics.

Tu, X., and M. S. Zhdanov, 2020, Robust synthetic aperture imaging of marine controlled-source electromagnetic data: IEEE Transactions on Geoscience and Remote Sensing, 1–13, doi: https://doi.org/10.1109/TGRS.2020.2966727.

Zhdanov, M. S., 2015, Inverse theory and applications in geophysics (second edition): Elsevier.

Zhdanov, M. S., A. Gribenko, and G. Wilson, 2012, Generalized joint inversion of multimodal geophysical data using Gramian constraints: Geophysical Research Letters, **39**, doi: https://doi.org/10.1029/2012GL051233.

Zhu, Y., 2017, Joint inversion of potential field and electromagnetic data using Gramian constraints: The University of Utah.